Scientific Research Publishing

Journal of Materials Science and Chemical Engineering, 2025, 13(8), 96-107
https://www.scirp.org/journal/msce
ISSN Online: 2327-6053
ISSN Print: 2327-6045

Electro-Assisted PDA/PEI Modified Membrane for Sustainable Separation of Anionic Dye

Chuan Yue[1], Menglei Han[2], Baoting Su[2], Kang Liu[2], Jianqiang Zhang[2*]

[1]School of Materials Science and Engineering, China University of Petroleum, Qingdao, China
[2]College of Science, China University of Petroleum, Qingdao, China
Email: *zhangjianqiang@upc.edu.cn

How to cite this paper: Yue, C., Han, M.L., Su, B.T., Liu, K. and Zhang, J.Q. (2025) Electro-Assisted PDA/PEI Modified Membrane for Sustainable Separation of Anionic Dye. *Journal of Materials Science and Chemical Engineering*, **13**, 96-108.
https://doi.org/10.4236/msce.2025.138008

Received: July 18, 2025
Accepted: August 26, 2025
Published: August 29, 2025

Abstract

The discharge of dye wastewater poses a serious threat to the environment and human health. Membrane separation technology based on electrostatic adsorption is considered an effective method for dye removal. However, its long-term application is hindered by the saturation of adsorption sites. In this study, an anionic dye-adsorbing membrane was fabricated via a co-deposition strategy, combined with patterned silver gel to impart conductivity. Acting as a cathode, the membrane electrolyzes water to generate OH^- ions at the interface that deprotonate the functional groups, thereby releasing the adsorbed dyes in situ. The membrane exhibits excellent dye rejection performance and enables sustainable separation over multiple cycles under this electro-assisted cleaning. This strategy avoids the use of additional reagents or secondary chemical pollutants, offering an efficient and sustainable membrane separation solution for the treatment of dye-containing wastewater.

Keywords

Membrane, Dye Separation, Adsorption, Electrolysis, Interfacial OH^-

1. Introduction

Organic dyes, owing to their vivid colors and chemical stability, are widely used across various industrial sectors, including textiles, plastics, food, rubber, inks, and paper manufacturing [1]-[3]. However, due to their inherently low utilization efficiency and the lack of effective control during discharge, large quantities of residual dyes are released into aquatic environments [4] [5]. This has posed serious threats to both ecosystems and human health [6]. Consequently, there is an urgent need to develop environmentally friendly and efficient water treatment technologies. For water-soluble reactive dyes, conventional biological and physicochemical

treatment often suffers from limited removal efficiency [7]. In contrast, membrane separation technology has emerged as a highly promising approach for dye wastewater treatment, due to its advantages such as environmental compatibility, low energy consumption, high separation efficiency, and ease of operation [8].

In membrane treatment of dye wastewater, the separation mechanisms typically involve size exclusion and selective permeation [9] [10]. Given that most industrial dyes have molecular weights below 1000 Da, nanofiltration membranes with molecular weight cut-off values in the range of 200 - 1000 Da are generally considered suitable for effective dye retention [11] [12]. However, the application of nanofiltration membranes is hindered by their high cost, relatively low water flux, and complex fabrication processes [13]. In recent years, adsorption-based membrane separation strategies have gained increasing attention for dye wastewater treatment [14]. This method incorporates adsorptive components into microporous membranes, enabling efficient dye capture through simple electrostatic interactions [15]. The functionalized microfiltration membranes possess high water flux, and their large-pore architecture provides abundant active adsorption sites, ensuring effective dye separation [16].

Despite the excellent separation performance exhibited by this strategy, it still suffers from notable limitations. During the adsorption process, the active sites on the membrane are gradually consumed [17]. Once adsorption saturation is reached, the membrane loses its effective rejection capacity, severely restricting its long-term operational stability [18]. Furthermore, the saturated membranes are typically difficult to regenerate and must be discarded, significantly increasing the overall cost of use. To address this issue, chemical desorption using highly concentrated alkaline solutions is often employed to partially restore the separation performance of the membrane [19]. However, this method involves complex operations and poses the risk of secondary pollution [20]. Therefore, achieving environmentally friendly in-situ regeneration of the membrane is challenging.

In this study, polydopamine (PDA) and polyethyleneimine (PEI) were co-deposited onto a commercial nylon microfiltration membrane, while a patterned conductive network was introduced to endow excellent electrical conductivity. Benefiting from electrostatic interactions, the modified membrane exhibited high adsorption capacity toward anionic organic dyes and demonstrated outstanding retention performance. During the separation process, the membrane functions as a cathode, where the electrolysis of water generates OH^- ions at the interface. These OH^- ions induce the deprotonation of functional groups and facilitate dye desorption, thereby enabling in-situ cleaning and performance recovery of the membrane. This strategy avoids secondary pollution and ensures efficient and stable dye separation over multiple cycles, highlighting its promising application potential in the treatment of dye wastewater.

2. Material and Methods

2.1. Materials

Polyethyleneimine (PEI, Mw = 600), tris(hydroxymethyl) aminomethane hydro-

chloride (Tris HCl, 99.9%), methylene blue (MB), methyl orange (MO), rhodamine B (RhB), and crystal violet (CV) were obtained from Aladdin Chemistry Co. Ltd., Shanghai, China. Dopamine hydrochloride (DPA, 98%), anhydrous sodium sulfate, anhydrous ethanol, sodium hydroxide (NaOH) were purchased from Macklin Biochemical Co., Ltd. (Shanghai, China). Nylon membrane (pore size: 0.45 μm), pH indicators, and platinum electrodes were commercially available. All the reagents were used as received without further purification.

2.2. Fabrication of Modified Membrane

The commercial nylon membranes were first ultrasonically cleaned in ethanol and deionized water for 10 min. The cleaned membranes were then immersed in 2 g/L dopamine hydrochloride and PEI solution, with the pH adjusted to 8.5 using a Tris-HCl buffer. A polydopamine/polyethyleneimine (PDA/PEI) functional layer was co-deposited onto the membrane by gentle stirring for 24 hours. Afterward, the membranes were rinsed three times with deionized water and dried at 60˚C. Subsequently, a patterned conductive network was constructed on the membrane surface using a commercially available conductive silver gel to impart electrical conductivity, yielding the final membrane referred to as E-NPP.

2.3. Characterization

The morphology of the membrane was examined via field-emission scanning electron microscopy (FESEM, JEOL JSM-6500, Japan) operated at 10.0 kV. The surface chemical composition was investigated by ATR-FTIR (Nicolet iN10 spectrometer, Thermo Scientific, USA) and XPS (AXIS-ULTRADLD-600 W, Al Kα). The contact angles of oil and water were tested using a JC2000 meter.

2.4. Dyes Adsorption Measurements

The dye concentrations were determined using a UV–vis spectrophotometer (UV-1601, Shimadzu, Japan). The characteristic UV–vis absorption peaks of the four dyes used in this study were 626 nm for MB, 464 nm for MO, 554 nm for RhB, and 590 nm for CV. The initial dye concentration was 10 mg/L, and the adsorption capacity and removal efficiency were calculated using the following equations:

$$\alpha = \frac{C_0 - C_1}{C_0} \times 100\% \tag{1}$$

where α represents the removal efficiency of dye, C_0 and C_1 are the concentrations in the solution before and after adsorption, respectively.

To further investigate the adsorption performance, equilibrium adsorption capacity (Q_e) tests were conducted. The modified membranes (0.1084 g) were immersed in 50 mL dye solutions with an initial concentration of 10 mg/L and maintained for 24 h to ensure adsorption equilibrium. The equilibrium adsorption capacity was calculated using the following equation:

$$Q_e = \frac{(C_0 - C_e) \times V}{M} \tag{2}$$

where Q_e (mg·g^{-1}) is the equilibrium adsorption capacity, C_0 (mg·L^{-1}) and C_e (mg L^{-1}) are the initial dye concentration and the concentration after 24 hours of equilibrium, respectively. V (L) is the volume of the dye solution, and M (g) refers to the weight of the modified membrane used in the test.

To understand the adsorption performance of the membrane, pseudo-first-order and pseudo-second-order kinetic models were employed to analyze the adsorption behavior. Their linear equations are as follows:

$$\ln(Q_e - Q_t) = \ln Q_{e1} - k_1 t \tag{3}$$

$$\frac{t}{Q_t} = \frac{1}{K_2 Q_{e2}^2} + \frac{1}{Q_{e2}} t \tag{4}$$

where Q_t and Q_e denote the adsorption capacities at time t and at equilibrium, respectively (mg/g). Q_{e1} and Q_{e2} represent the theoretical equilibrium adsorption capacities (mg/g) obtained by fitting the pseudo-first-order and pseudo-second-order kinetic models. K_1 and K_2 correspond to rate constants (min^{-1}) for pseudo-first-order and pseudo-second-order kinetics.

To further investigate the adsorption characteristics of the modified membrane, Langmuir and Freundlich isotherm models were used to describe the equilibrium distribution of various dye molecules at the solid–liquid interface. The linearized forms of the Langmuir and Freundlich isotherm equations are as follows:

$$\frac{C_e}{Q_e} = \frac{C_e}{Q_m} + \frac{1}{Q_m K_L} \tag{5}$$

$$\ln Q_e = \frac{\ln C_e}{n} + \ln K_F \tag{6}$$

In the equations, C_e denotes the concentration of solution at adsorption equilibrium (mg/L); Q_e and Q_m refer to the experimentally determined maximum adsorption capacity and the theoretical equilibrium adsorption capacity (mg/g), respectively. K_L and K_F are the equilibrium constants of the Langmuir and Freundlich adsorption models, respectively. The parameter n represents the intensity factor in the Freundlich model; when $n < 0.5$, the adsorption process is considered unfavorable, whereas an n value between 2 and 10 indicates favorable adsorption conditions.

The separation factor (R_L) is defined by the Langmuir model, and its equation expression is:

$$R_L = \frac{1}{1 + K_L C_0} \tag{7}$$

C_0 represents the initial solute concentration before adsorption (mg/L). The separation factor R_L indicates the nature of the adsorption process: $0 \le R_L < 1$ suggests favorable adsorption, $R_L = 1$ corresponds to a linear (reversible) adsorption, and $R_L > 1$ implies an unfavorable or irreversible adsorption process.

2.5. Separation Performance

A dead-end filtration system was used to assess separation efficiency, with the membrane connected to the cathode of a DC power supply and a platinum anode was positioned 50 mm above it. The effective filtration area was a circle with a diameter of 40 mm. In the cyclic separation experiment, an electric field was applied for 10 min after every 60 min of separation to release interfacial OH^-. The flux (J) and rejection rate of the membrane were calculated using the following equations, respectively:

$$J = \Delta V \Big/ \left(A_{ef} \times \Delta T \right) \tag{8}$$

$$R = \frac{C_1 - C_2}{C_1} \times 100\% \tag{9}$$

where A_{ef} denotes the effective membrane filtration area, ΔV represents the volume of filtrate collected over the set duration ΔT. C_1 and C_2 were the dye content before and after filtration, respectively.

3. Results and Discussion

3.1. Characteristics of Membranes

The morphological of the membrane was characterized by SEM. As shown in **Figure 1(ai)**, the commercial nylon membrane exhibited an irregular porous structure, which could provide abundant channels for the loading of adsorptive materials. After the co-deposition of PDA and PEI, the membrane turned brown, while its surface morphology remained largely unchanged and the porous structure was still clearly visible (**Figure 1(aii)**). Furthermore, the incorporation of conductive network imparted electrolytic functionality to the membrane. The ATR-FTIR spectra of the modified membrane (**Figure 1(b)**) exhibit absorption peaks at 3290 cm^{-1} and 1538 cm^{-1}, corresponding to the co-stretching vibrations of amino groups [21]. In addition, the peak at 1640 cm^{-1}, attributed to the C=N stretching vibration, confirms the presence of imine linkages formed through the interaction between PDA and PEI [22]. As shown in **Figure 1(c)**, the membrane consists of three elements (C, N, and O), but their relative proportions change after modification, with the content of N element increasing from 7.72% to 9.24%. Further analysis of the N 1s spectra reveals that only C–N bonds are present in the pristine nylon membrane (**Figure 1(d)**), whereas the modified membrane additionally exhibits C=N bonds (**Figure 1(e)**), confirming the successful preparation of the modified membrane [23].

Figure 1(f) shows the working mechanism of the electrolyzable membrane. Functioning as a cathode, the membrane electrolyzes water at the interface, generating OH^- ions and bubbles. The bubbles detach from the surface, while the OH^- ions diffuse outward, altering the interfacial pH to values exceeding 13. Under an applied voltage of 15 V, the diffusion range of OH^- ions expands with increasing time, reaching a distance of 3 cm from the interface within just 2 min (**Figure 1(g)**). Furthermore, the prepared membrane also exhibits superwettability,

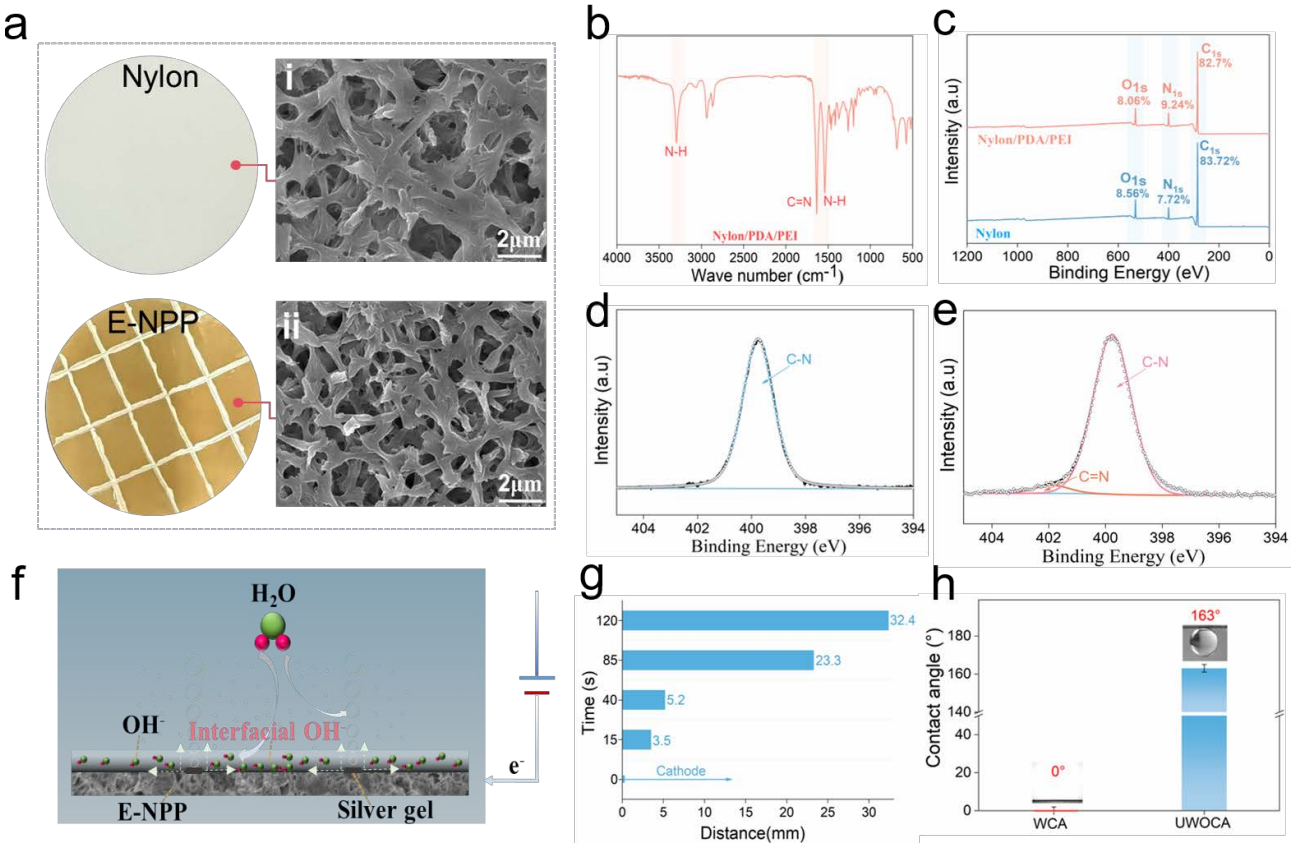

Figure 1. (a). Photographs and SEM images of the pristine nylon membrane (i) and the modified membrane (ii). (b). FTIR spectrum of the modified membrane. (c). XPS spectra and elemental composition of the pristine and modified membrane. (d), (e). Detailed XPS spectra of N1s for the pristine d and modified e membranes. (f). Schematic diagram of the mechanism of interfacial alkali release from a conductive cathode membrane. (g). The relationship between the diffusion distance of OH^- ions and time at 15V. (h). Water contact angle and underwater oil contact angle of the modified membrane.

with a water contact angle of 0˚ and an underwater oil contact angle of 163˚ (**Figure 1(h)**).

3.2. Dye Adsorption of Membrane

To evaluate the adsorption performance of the modified membrane, saturation adsorption experiments were conducted using four representative dyes. Among them, MB and MO serve as typical anionic dyes, while RhB and CV represent cationic dyes. The results reveal that the membrane achieves saturated adsorption capacities of 5.115 mg/g for MB and 4.019 mg/g for MO, in contrast to only 0.43 mg/g for RhB and 0.387 mg/g for CV (**Figure 2(a)**). These results show that the membrane can efficiently adsorb anionic dyes. Moreover, the adsorption mechanism was investigated using adsorption kinetic models. As shown in **Figure 2(b)** and **Figure 2(c)**, the correlation coefficients (R^2) of both the pseudo-first-order and pseudo-second-order kinetic models for MB adsorption are close to 1, indicating that the adsorption behavior of the membrane aligns well with both models. Therefore, in addition to physical adsorption, chemical adsorption also plays a significant role in the dye adsorption process. Furthermore, adsorption isotherm

experiments were performed for MB at initial concentrations of 10, 20, 30, 40, 50, and 60 mg/L. The fitting results (**Figure 2(d)** and **Figure 2(e)**) show that the Langmuir isotherm model yields a higher R^2 compared to the Freundlich model, indicating that the adsorption process of the modified membrane is more consistent with monolayer chemical adsorption on a homogeneous surface. According to Equation 7, the corresponding separation factor (RL) values were 0.294, 0.178, 0.129, 0.105, 0.087, and 0.076, respectively. All RL values fall within the range of (0, 1), confirming the adsorption process is completely feasible. The decreasing RL values at higher initial concentrations further show that the adsorption process is highly favorable at elevated concentrations, which is fully consistent with the monolayer chemical adsorption mechanism of the Langmuir model. In **Figure 2(f)**, the saturated adsorption capacity remains nearly unaffected in the presence of 0.1 mol/L sodium sulfate solution, confirming the feasibility of electrochemical applications.

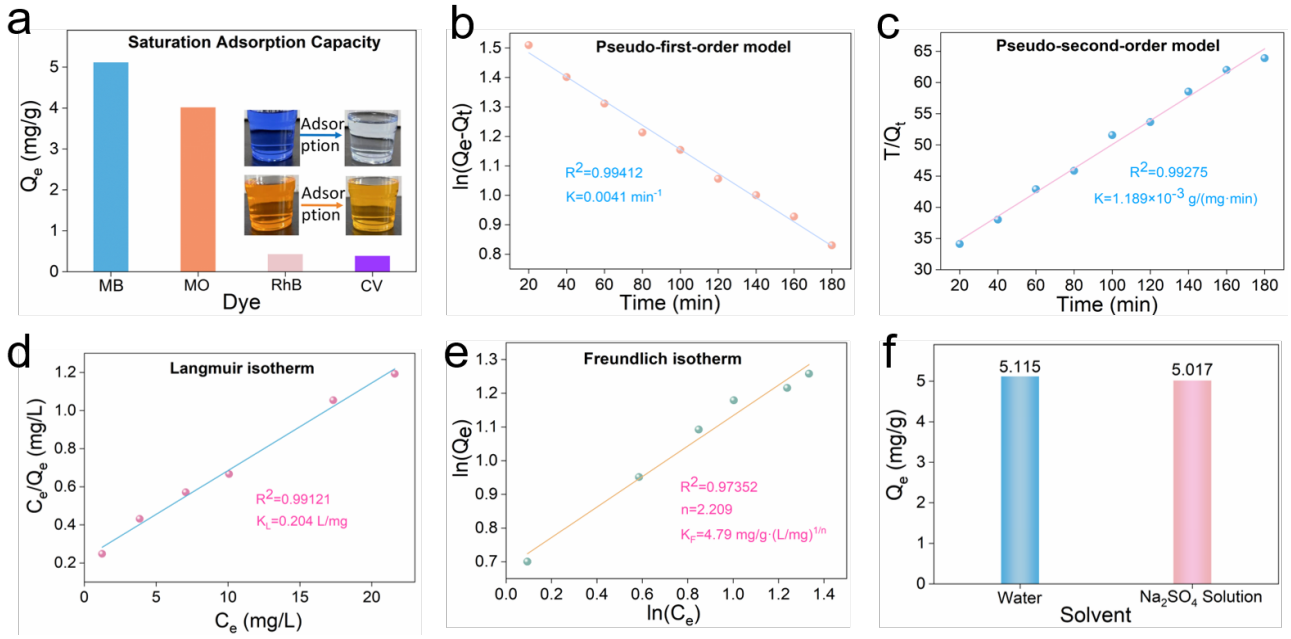

Figure 2. (a). Saturated adsorption capacities of the modified membrane for MB, MO, RhB, and CV dyes. (b). Pseudo-first-order adsorption kinetic curve of MB. (c). Pseudo-second-order adsorption kinetic curve of MB. (d). Langmuir adsorption isotherm curve of MB. (e). Freundlich adsorption isotherm curve of MB. (f). Saturated adsorption capacity of the modified membrane for MB in pure water and 0.1 mol/L Na_2SO_4 solution.

3.3. Dye Separation of Membrane

The dye rejection performance of the E-NPP membrane was evaluated using a homemade filtration device (**Figure 3a**). The membrane was connected to the negative electrode of a DC power supply, while the platinum sheet electrode above the membrane was linked to the positive electrode, and the separation process was conducted under gravity-driven conditions. As shown in **Figure 3b**, the dye rejection mechanism of the membrane is attributed to electrostatic adsorption. Both PDA and PEI contain abundant amino groups, which are protonated in aqueous

solution and thus carry positive charges. Dyes with opposite charges will generate electrostatic attraction at the solid-liquid interface, causing dye molecules to be firmly bound to the surface or pores. This electrostatic interaction enables the membrane to selectively permit the passage of water while effectively retaining anionic dyes. In **Figure 3(c)**, the membrane exhibits a separation flux of 77.2 ± 5 $L \cdot m^{-2} \cdot h^{-1}$ over an extended period. Initially, the rejection rate of MB exceeded 99.8% and remained stable for up to 70 min, showing excellent separation efficiency (**Figure 3(c)**). The dye solution before filtration appeared dark blue and showed a distinct absorption peak at 626 nm in the UV–vis spectrum (**Figure 3(d)**). After filtration, the permeate became clear and transparent with the absorption peak disappearing, and the filtration area of the membrane visibly turned blue (**Figure 3(d)**). These results confirm that the modified membrane can effectively retain anionic dyes. However, after 80 min of continuous filtration, the rejection rate decreased to 85.3%, showing a downward trend. As the separation time extended to 90 min, the rejection rate further declined to 72.7% (**Figure 3(c)**), suggesting that the membrane gradually lost its effective separation capability with prolonged use. This decline is attributed to the saturation of adsorption and there are no remaining adsorption sites to retain dyes.

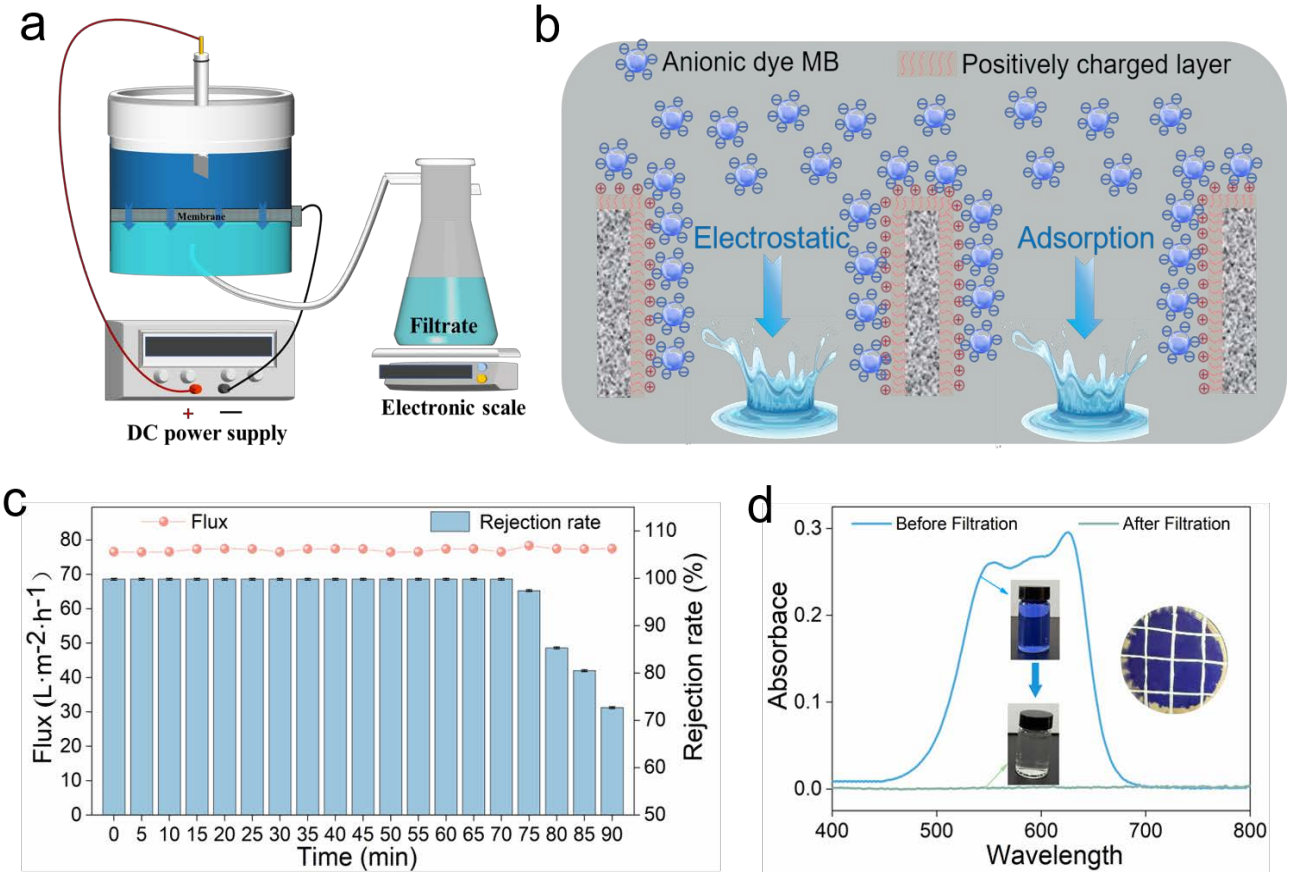

Figure 3. (a). Schematic diagram of the dye separation apparatus. (b). Schematic illustration of the mechanism for anionic dye rejection by the modified membrane. (c). Time-dependent changes in flux and dye rejection rate during the separation process. (d). UV absorbance and photographs of MB before and after separation.

3.4. Sustainable Separation of Dyes

To address the issue of the inability to maintain the long-term performance of the membrane, a periodic electrolysis strategy was introduced during the separation process. Specifically, after every 1 h of separation, the in situ electrolysis was performed for 10 min under 15 V voltage. During electrolysis, the interfacial OH^- deprotonates the charged functional groups, rendering them neutral. This change weakens the electrostatic interactions between the membrane and the adsorbed dye molecules, thereby enabling their release and achieving in situ membrane cleaning. As shown in **Figure 4(a)**, over six separation cycles, the membrane consistently maintained both high rejection rates and stable flux. The average rejection rate in each cycle remained above 99.8% (**Figure 4(c)**), showing the membrane achieved sustainable separation. The desorption process was further investigated by observing the electrolysis of the filtered membrane. After 5 min of electrolysis, the initially colorless solution turned blue, and the color deepened further after 10 min. This shows that the dyes adsorbed on the membrane were

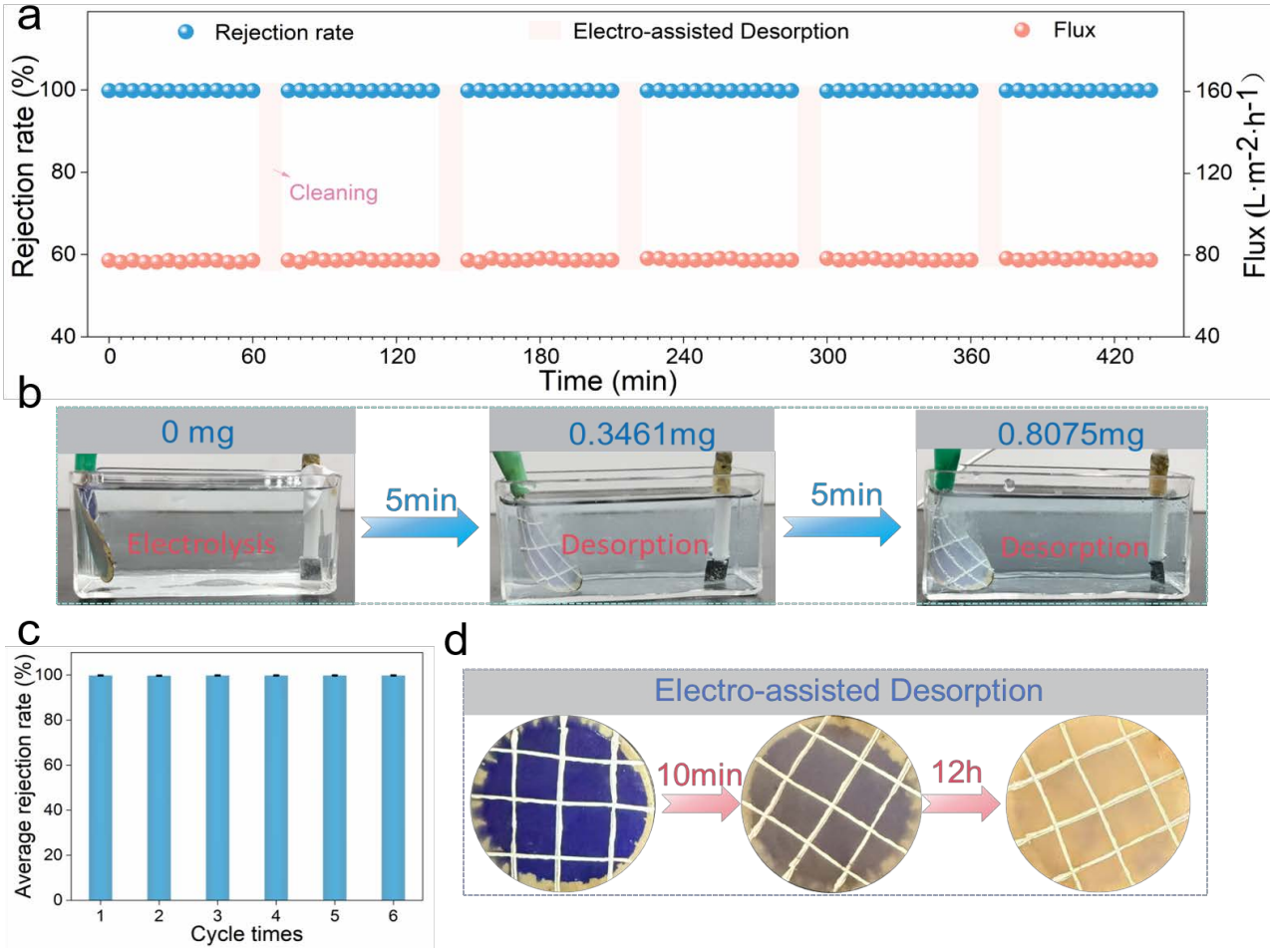

Figure 4. (a). Changes in flux and rejection rate of MB during multi-cycle continuous separation under electro-assisted cleaning. (b). Images of MB release during the cleaning process. (c). Average MB rejection rate of the membrane over six cycles. (d). Time-dependent images of dye desorption efficiency under electro-assisted cleaning.

gradually stripped off during electrolysis, with the released amounts reaching 0.3461 mg and 0.8075 mg (**Figure 4(b)**), respectively. Consequently, the adsorption sites on the membrane were regenerated, allowing it to continue performing separations effectively. Furthermore, as shown in **Figure 4(d)**, the membrane color changed from dark blue to light blue after 10 min of electrolysis. Notably, after 12 h of continuous electrolysis, the adsorbed dye was almost completely desorbed from the membrane. These results clearly demonstrate that short-term electrolysis enables multi-cycle continuous dye separation, while prolonged electrolysis facilitates complete membrane regeneration. Unlike conventional regeneration methods that rely on high concentrations of alkali, this electrochemical strategy generates interfacial OH^- ions that are neutralized by H^+ ions produced at the anode, resulting in a neutral filtrate. This process avoids additional chemical contamination and eliminates the need for external chemical additives.

4. Conclusion

In summary, the electrolyzable E-NPP membrane was successfully fabricated by co-depositing a PDA/PEI functional layer and combining a patterned conductive network. This membrane exhibits excellent adsorption performance for anionic dyes MB and MO, with saturated adsorption capacities of 5.115 mg/g and 4.019 mg/g, respectively. Its adsorption behavior conforms to both the first-order and second-order kinetic models, as well as the Langmuir isothermal adsorption model. Furthermore, the membrane achieves a rejection rate of over 99.8% for anionic dyes. After filtration, the adsorbed dye molecules can be *in-situ* desorbed via interface OH^- generated by electrolysis. With the assistance of interface OH^-, the membrane maintains efficient rejection performance over 6 cycles (totaling 360 min), significantly enhancing its long-term separation capability. This strategy requires no additional chemical reagents and avoids secondary pollution, significantly enhancing separation efficiency.

Acknowledgements

This work was supported by the Taishan Scholar Young Talent Program (tsqn202211083), Shandong Provincial Natural Science Foundation (ZR2022ME046), Youth Innovation Team Plan Project for Higher Education Institution of Shandong Province (2023KJ072), Natural Science Foundation of Shandong Province (ZR2024QE127) and Fundamental Research Funds for the Central Universities (24CX03006A).

Conflicts of Interest

The authors declare no conflicts of interest regarding the publication of this paper.

References

[1] Pallot, H., Isloor, A.M. and Ismail, A.F. (2025) Effective Separation of Agrochemicals and Textile Dyes from Polluted Aqueous Solution Employing Ternary ZnCoFe Layered

Double Hydroxide Incorporated Polyethersulfone Hollow Fiber Ultrafiltration Membrane. *Chemical Engineering Journal*, **520**, Article 165254. https://doi.org/10.1016/j.cej.2025.165254

[2] Liu, C., Zhu, L., Zhang, Y., Hu, W., Shen, Y., Jin, H., *et al.* (2025) Facile Fabrication of High-Performance Membrane with 2D GO Nanosheet in Membrane Skin by Pic-Assisted NIPS Method for Dye/Salt Separation. *Journal of Membrane Science*, **733**, Article 124339. https://doi.org/10.1016/j.memsci.2025.124339

[3] Liu, Y., Luo, F., Zheng, K. and Zhou, S. (2025) Novel Polyfurfuryl Alcohol Loose Nanofiltration Membrane for Efficient Dye/Salt Selective Separation. *Environment International*, **202**, Article 109622. https://doi.org/10.1016/j.envint.2025.109622

[4] Wu, D., li, H., Pan, G., Wang, M., Yu, W., Wang, G., *et al.* (2024) Sustainable Superwetting Membrane for Effective Separation of Oil-Water Emulsion and Dye Removal. *Separation and Purification Technology*, **343**, Article 127084. https://doi.org/10.1016/j.seppur.2024.127084

[5] Wang, Z., Yuan, S., Wang, D., Zhang, N., Shen, Y. and Wang, Z. (2025) n-Oxide Zwitterionic-Based Antifouling Loose Nanofiltration Membranes with Superior Water Permeance and Effective Dye/Salt Separation. *Environmental Science & Technology*, **59**, 5856-5865. https://doi.org/10.1021/acs.est.5c00916

[6] Yao, N., Ji, S., Xing, Y., Chen, J., Cheng, Y., Ruan, X., *et al.* (2025) Green Resource Utilization of Textile and Dyeing Wastewater: Fabrication of a Chlorine-Resistant ZIF-L/PDA Loose Nanofiltration Membrane via Interfacial Polymerization and Its Performance in Dye/Salt Separation. *Separation and Purification Technology*, **377**, Article 134193. https://doi.org/10.1016/j.seppur.2025.134193

[7] Liu, X., Zhang, J., Wu, H., Li, F., Liu, Z., Ma, Y., *et al.* (2025) Synergistic Antifouling PBI Nanofiltration Membrane via Ag@UiO-66-NH_2 Immobilization and Hydrophilic Polymer Brush Grafting for Dye/Salt Separation. *Desalination*, **613**, Article 119067. https://doi.org/10.1016/j.desal.2025.119067

[8] Liu, Y., Zhu, J., Chi, M., Eygen, G.V., Guan, K. and Matsuyama, H. (2025) Comprehensive Review of Nanofiltration Membranes for Efficient Resource Recovery from Textile Wastewater. *Chemical Engineering Journal*, **506**, Article 160132. https://doi.org/10.1016/j.cej.2025.160132

[9] Hao, J., Li, J., Wang, L., He, M., Wang, J., Wang, X., *et al.* (2025) Electrically Induced Modulation of Pore Size and Surface Potential in Conductive Nanofiltration Membranes for Enhanced Dye/Salt Selective Separation. *Journal of Membrane Science*, **724**, Article 123993. https://doi.org/10.1016/j.memsci.2025.123993

[10] Li, H., Xiao, S., Zhao, X., Yuan, J. and Yu, S. (2025) Preparation of High-Flux Loose Nanofiltration Membranes for Efficient Dye/Salt Separation by Controlling Interface Polymerization through Physical and Chemical Dual Constraints. *Separation and Purification Technology*, **362**, Article 131720. https://doi.org/10.1016/j.seppur.2025.131720

[11] Li, R., Cao, S., Feng, X., Don, J., Guo, X., Wang, H., *et al.* (2022) Guanidinium-Based Loose Nanofiltration Membranes for Dye Purification and Chlorine Resistance. *Separation and Purification Technology*, **300**, Article 121941. https://doi.org/10.1016/j.seppur.2022.121941

[12] Nie, M.X., Zheng, Z., Song, F., Lu, J. and Zhan, X. (2025) Construction of Highly Permeable Polyhedral Oligomeric Silsesquioxanes/Polyamide Nanofiltration Membranes via Liquid-Solid Interfacial Polymerization for Dye Desalination. *Journal of Membrane Science*, **733**, Article 124293. https://doi.org/10.1016/j.memsci.2025.124293

[13] Yu, W., Liu, Y., Xu, Y., Li, R., Chen, J., Liao, B.Q., *et al.* (2019) A Conductive PVDF-Ni Membrane with Superior Rejection, Permeance and Antifouling Ability via Electric Assisted *In-Situ* Aeration for Dye Separation. *Journal of Membrane Science*, **581**, 401-412. https://doi.org/10.1016/j.memsci.2019.03.083

[14] Kim, Y.J., Jang, J.K., Yoo, S.Y., Lee, J. and Park, H.B. (2025) Enhanced Dye Adsorption and Separation Using Iterative Growth of Sulfonated UiO-66 on PTFE Membranes. *Journal of Membrane Science*, **719**, Article 123731. https://doi.org/10.1016/j.memsci.2025.123731

[15] Hui, Q., Diao, Y., Li, Z., Wang, F., Guan, Z., Wang, C., *et al.* (2025) Organic–Inorganic Mixed Matrix Membrane Constructed by Chitosan and Red Mud Based γ-AlOOH Hierarchical Porous Microspheres as Superior Adsorbents for Anionic Dye and Microplastics. *Separation and Purification Technology*, **371**, Article 133245. https://doi.org/10.1016/j.seppur.2025.133245

[16] Gupta, K., Yasa, S.R., Khan, A., Sharma, O.P. and Khatri, O.P. (2022) Charge-Driven Interaction for Adsorptive Removal of Organic Dyes Using Ionic Liquid-Modified Graphene Oxide. *Journal of Colloid and Interface Science*, **607**, 1973-1985. https://doi.org/10.1016/j.jcis.2021.10.017

[17] Wan, H., Zhu, X., Wang, J., Cao, F., Zhang, Y., Yao, Z., *et al.* (2025) Adsorptive Nanofibrous Membranes for Bidirectional Removal of Cationic and Anionic Dyes. *Separation and Purification Technology*, **361**, Article 131515. https://doi.org/10.1016/j.seppur.2025.131515

[18] Qi, Y., Chen, Y., Liu, H., Zhao, J., Yu, Y., Wang, R., *et al.* (2024) Construction of Highly Hydrophilic PAN-co-IA/CNTs@TA Composite Membrane with Large Flux and High Retention for Purification of Dye Wastewater. *Chemical Engineering Journal*, **487**, Article 150752. https://doi.org/10.1016/j.cej.2024.150752

[19] Fang, J., Chen, Y., Fang, C. and Zhu, L. (2022) Regenerable Adsorptive Membranes Prepared by Mussel-Inspired Co-Deposition for Aqueous Dye Removal. *Separation and Purification Technology*, **281**, Article 119876. https://doi.org/10.1016/j.seppur.2021.119876

[20] Gan, S., Li, H., Zhu, X., Liu, X., Wei, K., Zhu, L., *et al.* (2023) Constructing Scalable Membrane with Tunable Wettability by Electrolysis-Induced Interface pH for Oil-water Separation. *Advanced Functional Materials*, **33**, Article 2305975. https://doi.org/10.1002/adfm.202305975

[21] Zhou, Q., Liu, S., She, J., Wang, X., Lu, X. and Wu, C. (2022) In-Situ Aeration-Assisted Polydopamine/Polyethyleneimine Copolymerization and Deposition for Rapid and Uniform Membrane Modification. *Journal of Membrane Science*, **657**, Article 120662. https://doi.org/10.1016/j.memsci.2022.120662

[22] Li, Z., Hu, K. and Feng, X. (2021) Concentration of Potassium Acetate Solutions via Sweeping Gas Pervaporation Using TFC Membranes Comprising of a PDA Sublayer and PEI/PAA Bilayers. *Separation and Purification Technology*, **277**, Article 119429. https://doi.org/10.1016/j.seppur.2021.119429

[23] Shi, X., Zhang, Q., Wang, Z., Bi, Q. and Lin, Y. (2025) Acetone-Modulated Reverse Interfacial Polymerization Was Employed to Prepare PEI/PDA Positively Charged Composite Nanofiltration Membranes for Mg^{2+}/Li^{+} Separation. *Journal of Membrane Science*, **720**, Article 123780. https://doi.org/10.1016/j.memsci.2025.123780